Nano Research 2018, 11(7): 3762–3770
https://doi.org/10.1007/s12274-017-1947-y
Research Article
ISSN 1998-0124
CN 11-5974/O4

Phytochemical-encapsulated nanoplatform for "on-demand" synergistic treatment of multidrug-resistant bacteria

Panpan Sun[1,3], Yan Zhang[1], Xiang Ran[1], Chaoying Liu[2] (✉), Zhenzhen Wang[1], Jinsong Ren[1] (✉), and Xiaogang Qu[1] (✉)

[1] *State Key Laboratory of Rare Earth Resources Utilization and Laboratory of Chemical Biology, Changchun Institute of Applied Chemistry, Chinese Academy of Sciences, Changchun 130022, China*
[2] *Department of Respiratory Medicine, First Affiliated Hospital, Jilin University, Changchun 130021, China*
[3] *University of Science and Technology of China, Hefei 230029, China*

Received: 9 October 2017
Revised: 29 November 2017
Accepted: 1 December 2017

KEYWORDS
multidrug-resistant bacteria,
nanocarriers,
on-demand,
synergistic treatment

ABSTRACT

Though phytochemicals are a promising alternative to traditional antibiotics for combating resistant bacteria, the low water solubility and lack of selectivity seriously hinder their widespread applications. Herein, we constructed a hyaluronidase-activated "on-demand" delivery nanocarrier to encapsulate plant essential oils (PEOs) for the synergistic treatment of multidrug-resistant bacteria. The bioavailability and selectivity of PEOs was enhanced and the antibacterial effect was significantly improved by combining with the photothermal effect of the nanocarrier. This antibacterial system was successfully applied for healing methicillin-resistant *Staphylococcus aureus*-infected wound with negligible cytotoxicity and biotoxicity in mice. Given the increasing risk of antibiotic resistance, we believe that this phytochemical-encapsulated nanoplatform would provide a long-term solution and be a new powerful tool for skin-associated bacterial infections.

1 Introduction

Over the past decades, bacterial infectious diseases are undoubtedly one of the biggest threats to public health, globally [1]. Since antibiotics were discovered in the 1940s, these "miracle drugs" have saved countless lives [2]. However, the continued effectiveness of antibiotics has been severely threatened in recent years [3]. The overuse of antibiotics leads to the emergence of multidrug-resistant (MDR) strains, known as superbugs [4]. Meanwhile, residues of antibiotics in humans, animal products, and the environment increase the genotypic and phenotypic variability of bacteria and accelerate the emergence of MDR microbes

Address correspondence to Chaoying Liu, cyliu293a@163.com; Jinsong Ren, jren@ciac.ac.cn; Xiaogang Qu, xqu@ciac.ac.cn

[5, 6]. The MDR bacteria are resistant to numerous conventional antibiotics and lead to higher mortality in clinics annually [7]. One possible way to combat the acute health crisis of drug-resistance is the design of new antibiotics [8]. Discouragingly, the development of new antibiotics has been restricted over the past decades, and the inevitable evolution of new resistance strains will eventually invalidate the newly introduced antibiotics [9]. Therefore, the development of alternative and effective antimicrobial agents to eliminate the MDR strains is urgently needed.

Phytochemicals, compounds extracted from plants and responsible for their defense response against pathogenic infection, have emerged as effective alternatives to conventional antibiotics for treating MDR bacteria and biofilms [10, 11]. Currently, these plant essential oils (PEOs) have attracted great interest as "green" bactericides because of their powerful antibacterial activities and excellent biocompatibility [12–14]. Compared with traditional synthetic antibiotics, PEOs have several distinctive advantages: a) They exhibit broad-spectrum bactericidal properties through complex mechanisms, which are difficult for bacteria to develop resistance against [14, 15], b) they are non-toxic to vertebrates within antibacterial concentrations and could be easily metabolized and biodegraded, hence are beneficial for decreasing the bacterial variability [16, 17], and c) these natural compounds derived from plants are easily acquired and widely available, providing a large inventory for new antiseptics [18]. Though promising, the antibacterial activity of most PEOs is weaker than that of the common antibiotics, and high doses of PEOs are needed for exhibiting potent bactericidal effect [15]. Moreover, poor solubility in aqueous solutions and non-selectivity of PEOs for some infections consequently cause very low bioavailability and decrease the therapeutic effects, which seriously hinders their widespread applications [19–22]. Recently, several approaches have been reported to enhance their aqueous stability, such as packing PEOs into surfactant- [23] or nanoparticle-stabilized colloidal delivery systems [11] and molecular inclusion complexes [24]. Nevertheless, these strategies may suffer disadvantages such as colloidal instability, non-selectivity, and low PEO loading capacity, which significantly impair their practical use *in vivo*.

Nowadays, nanoparticle-based "on-demand" drug delivery systems have attracted considerable attention since they dramatically improve the therapeutic efficacy at targeted sites [25–28]. Among the numerous control-release nanocarriers, mesoporous silica-coated gold nanorod (AuMP)-based system provides an ideal platform owing to their high photothermal efficiency, large loading capacity, splendid biocompatibility, and great chemical stability [29–32]. Inspired by these unique features, for the first time, we used the surface-modified AuMP as a carrier to encapsulate the PEOs. Cinnamaldehyde (CA), a major PEO extracted from cinnamon, shows broad bactericidal ability against both gram-positive and gram-negative microbes, even MDR bacteria [33, 34]. Moreover, it has been given the generally recognized as safe (GRAS) status in the USA. In this study, CA was used as a plant bactericidal agent. As a non-toxic extracellular polysaccharide, hyaluronic acid (HA) could be readily biodegraded by hyaluronidase (Hyal), which is overexpressed in numerous bacteria [35, 36]. Hence, HA was chosen as the capping and "on-demand" releasing agent in response to the overexpressed Hyal in bacteria-infected sites. As illustrated in Scheme 1,

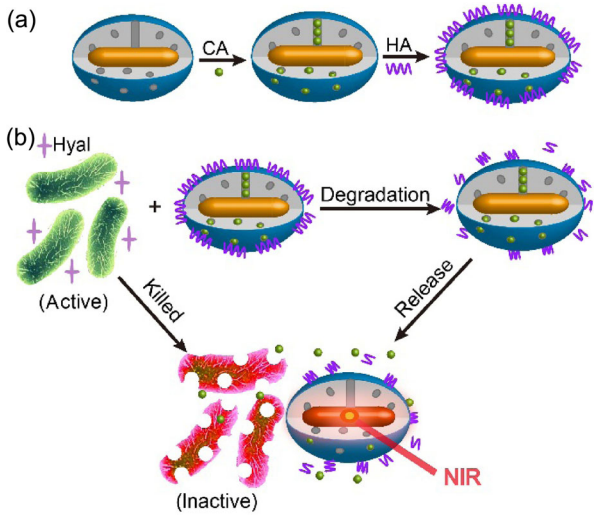

Scheme 1 (a) Preparation of the on-demand CA delivery nanoplatform CA@AuMN-HA. (b) Schematic illustration of the synergistic antibacterial mechanism. The loaded CA was released when the capping HA was degraded by Hyal-secreting bacteria. When combined with the photothermal effect of AuMN under NIR irradiation, this nanoplatform exhibited chemo-photothermal synergistic antibacterial effect.

AuMP was used as the carrier to encapsulate CA. The packaged CA could be released at the infection site when the capping HA was degraded by Hyal-secreting bacteria. This "on-demand" PEO delivery system, with large loading capacity and Hyal-triggered release behavior, could significantly improve the bioavailability and the selectivity of PEOs. Meanwhile, the synergistic photothermal effect of the nanocarrier could reduce the dosage and dramatically enhance the antibacterial efficacy of PEOs. Consequently, this antibacterial system was successfully applied for healing methicillin-resistant *Staphylococcus aureus* (MRSA)-infected wound.

2 Experimental

2.1 Reagents and materials

Tetrachloroauric acid ($HAuCl_4$), sodium borohydride ($NaBH_4$), tetraethyl orthosilicate (TEOS), ascorbic acid, silver nitrate ($AgNO_3$), and (3-aminopropyl) triethoxysilane (APTES) were obtained from Sigma-Aldrich. Cinnamaldehyde was purchased from Aladdin and cetyltrimethylammonium bromide (CTAB) was purchased from Alfa Aesar. Hyal was obtained from Shanghai Sangon Biological Engineering Technology & Services (Shanghai, China). All the chemicals were used without further purification. We used Milli-Q water (18.2 mΩ) to prepare all buffers in all experiments.

2.2 Preparation of chemically modified mesoporous silica-coated Au nanorods

The mesoporous silica-coated Au nanorods were synthesized according to that reported by us previously. First, 1.0 mL 0.20 M CTAB solution was mixed with $HAuCl_4$ (1.0 mL, 0.5 mM). Then, an ice-cold $NaBH_4$ solution (0.12 mL, 0.01 M) was added under sustained stirring to obtain the seed solution. The growth solution was prepared by mixing 100 mL 0.2 M CTAB, 5.6 mL 4 mM $AgNO_3$, 6.5 mL 23 mM $HAuCl_4$, and 95 mL Milli-Q water. Ascorbic acid (0.08 M) was slowly added to the mixture in a dropwise manner until the mixture became colorless. Finally, 1.8 mL seed solution was added to the growth solution at 27–30 °C. Then, the as-synthesized Au nanorods were centrifuged as 75 mL aliquots to remove excess CTAB surfactant. The precipitate was dispersed in 50 mL Milli-Q water and 500 μL 0.1 M NaOH solution was added upon stirring. Three 150 μL injections of TEOS (20%) methanol solution were added at 30 min intervals. The reaction mixture was reacted for 6 h to obtain AuMP. To obtain the amino-modified AuMP (AuMN), 10 μL APTES in 100 μL methanol was added to the reaction mixture under stirring for another 5 h. Then, the solution was centrifuged twice to obtain a red precipitate. To remove the surfactant template (CTAB), the precipitate was refluxed for 1 h in 20 mL methanol solution which contained 0.2 mL HCl (37%). The resulting surfactant-removed AuMN was placed under high vacuum to remove the remaining solvent in the mesopores.

2.3 CA loading and HA capping of AuMP

For CA loading, AuMN (20 mg) was soaked in an ethanolic solution of CA (200 mg) and stirred for 24 h. The nanoparticles were then centrifuged and washed with pure water to remove unloaded molecules. All the washing solutions were collected, and the loading of CA was evaluated by UV–Vis spectroscopy (Fig. S5 in the Electronic Supplementary Material (ESM)). The resulting AuMN was allowed to be capped with HA through 1-ethyl-3-(3-dimethylaminopropyl) carbodiimide/N-hydroxysuccinimide (EDC/NHS) chemistry. HA (30 mg) was dissolved in water and activated by using EDC (2 mg·mL^{-1}) and NHS (2 mg·mL^{-1}) in a 2-(N-morpholino) ethanesulfonic acid (MES) buffer (pH = 6.0). CA-loaded AuMN (15 mg) was added, stirred for 20 h, and then centrifuged to remove the untreated HA.

2.4 CA release experiments

The as-synthesized CA-loaded AuMN-HA materials (20 mg) were dispersed in 10 mL acetate buffer (pH = 5, containing 1.5‰ tween-20) with and without Hyal (150 U·mL^{-1}) at 37 °C. An acidic pH was chosen because it is suitable for Hyal activity and is consistent with the infection environment. Aliquots (100 μL) were taken from the suspension at predetermined time intervals, and then replaced with an equal volume of the fresh medium. The release of CA was monitored by the characteristic absorption peak of CA at

291 nm (Fig. S5 in the ESM). The concentrations of CA@AuMN-HA and Hyal were changed to study their influence on the CA-releasing efficiency (20 mg nanoparticles in 20 mL acetate buffer and Hyal 200 U·mL^{-1}, respectively) (Fig. S6 in the ESM).

2.5 Bacterial culture and antibacterial experiments

A monocolony of MRSA and drug-resistant *Escherichia coli* (*E. coli*) on the Luria–Bertani (LB) agar plate was transferred to 20 mL broth and incubated at 37 °C for 24 h with stirring at 180 rpm. Then, the bacteria were diluted with broth to 10^6 cfu·mL^{-1}. The obtained solution (500 μL) was mixed with different concentrations of (1) PBS (control), (2) free CA, (3) CA@AuMN-HA, (4) AuMN-HA + NIR, and (5) CA@AuMN-HA + NIR and incubated for 8 h. Here, NIR implies that the cells were irradiated at 808 nm (2.5 W·cm^{-2}) for 5 min. Then, the solutions of bacteria treated with 80 μg·mL^{-1} nanoparticles were plated on agar by spread plated method and cultured at 37 °C for 24 h. Free CA used in these experiments possessed equivalent concentrations of CA@AuMN-HA (80 μg·m L^{-1} CA@AuMN-HA could release nearly 7.2 μg·mL^{-1} CA after 8 h).

2.6 Mouse model of wound and histological analysis

To evaluate the potential of CA@AuMN-HA for treating wound infection, the injury model was developed on the backs of mice. The back of BALB/c mice (6–8-week-old) was slashed and injected with 1 × 10^6 MRSA cells to develop the infected wound model. The mice were divided into five groups (four mice per group)—(1) PBS (control), (2) free CA (7.2 μg·mL^{-1}), (3) CA@AuMN-HA (80 μg·mL^{-1}), (4) AuMN-HA + NIR, and (5) CA@AuMN-HA + NIR. The wounds were observed and photographed, and Band-Aids were changed at 24 h intervals. After 3 days of therapy, the mice were sacrificed to harvest the wound tissues. The wound tissues were placed in 1 mL sterile saline and homogenized. The obtained solutions were cultured at 37 °C overnight, and the bacterial count was determined by plate count method. For histological analysis, the harvested wound tissues were fixed in neutral buffered formalin, embedded into paraffin, sectioned into ~ 4-μm thick sections, and stained with hematoxylin and eosin (H&E). The histological analysis was performed at the college of Basic Medical Science of Jilin University. The samples were examined by an Olympus BX-51 microscope under bright field.

2.7 Methyl thiazolyl tetrazolium (MTT) assay for cytotoxicity

MC-3T3-E1 cells were seeded in 96-well assay plates (5,000 cells per well) and incubated for 24 h. Then the prepared samples with indicated concentrations of CA@AuMN-HA were added and further incubated for 24 h. To determine cytotoxicity, the medium was removed, washed with phosphate buffered saline (PBS), and 100 μL MTT solution was added to each well. The plate was incubated in the cell culture incubator for an additional 4 h. Next, the cells were lysed by the addition of 100 μL dimethylsulfoxide (DMSO). Absorbance values were determined using Bio-Rad model-680 microplate reader at 490 nm with 630 nm set as the reference wavelength. The experiment was performed in four replicates for each treatment group.

2.8 *In vivo* biosafety

The mice were topically treated with 80 μg·mL^{-1} CA@AuMN-HA and irradiated with NIR laser for 5 min, while mice in the control group were treated with PBS buffer. After observation for 3 days, the mice were sacrificed and six major organs (the heart, liver, spleen, lung, kidney, and brain) were harvested. These organs were fixed in neutral buffer formalin, embedded into paraffin, sectioned into ~ 4-μm thick sections, and stained with H&E. The histological analysis was performed at the college of Basic Medical Science of Jilin University. The samples were examined by an Olympus BX-51 microscope under bright field.

3 Results and discussion

AuMP was synthesized according to our previously reported method [30, 31]. Briefly, gold nanorods (GNRs) were first synthesized via a seed-mediated surfactant-directed method (Fig. S1 in the ESM). Subsequently, mesoporous silica was encapsulated on

the GNRs by the modified sol–gel approach to obtain AuMP (Fig. 1(a) and Fig. S1 in the ESM). Scanning electron microscopy (SEM) and transmission electron microscopy (TEM) images revealed that the average diameter of AuMP was 55 nm with a homogeneous silica shell of 15 nm. N_2 adsorption–desorption isotherms of the AuMP displayed a characteristic type IV isotherm. The average pore diameter was 2.4 nm with a narrow pore distribution (Fig. S2 in the ESM). Then, the AuMP was amine-modified to obtain AuMN. Finally, HA-capped AuMN was fabricated. As illustrated in Fourier transform infrared (FTIR) spectroscopy (Fig. 1(b)), the successful conjugation of HA onto AuMN was verified by the stretching vibrations around 1,407 and 1,635 cm^{-1} in AuMN-HA, which could be assigned to the C–N and amide C=O groups, respectively. The successful surface modification was also validated by TEM (Fig. 1(a)) and corresponding zeta potentials (Fig. 1(c)). The optical properties of GNR, AuMN, and AuMN-HA were studied by UV–Vis spectroscopy (Fig. S3 in the ESM). All the spectra showed a transverse plasmon resonance band around 520 nm and a longitudinal plasmon resonance band around 800 nm. To evaluate the photothermal effect of the carrier, the aqueous solution of AuMN-HA was exposed to continuous NIR irradiation at 808 nm for 10 min. As shown in Fig. S4 in the ESM, the increase in temperature of the solution was directly proportional to the increase in concentration of AuMN-HA.

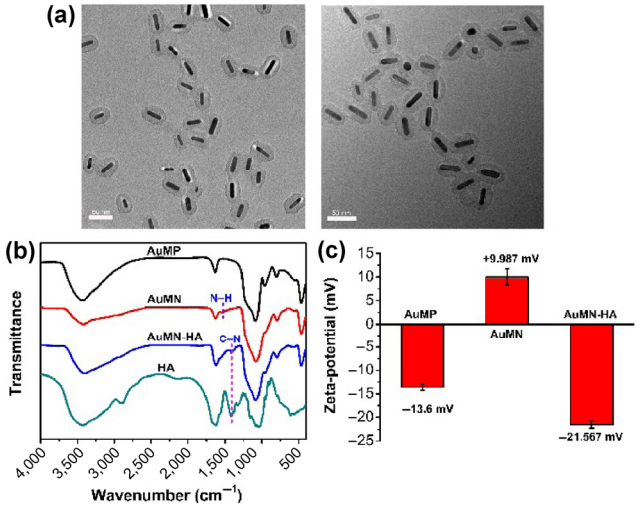

Figure 1 (a) TEM micrographs of AuMN (left) and AuMN-HA (right). (b) FTIR spectra of AuMP, AuMN, AuMN-HA, and HA. (c) The corresponding zeta potentials. Scale bar in (a) = 50 nm.

Next, we studied the loading efficiency and Hyal-activated release of the delivery system. The maximum loading ratio of CA was calculated to be 24% (Fig. S5 in the ESM). Hyal-activated drug release from the CA@AuMN-HA was monitored over 24 h in acetate buffer (pH = 5). As shown in Fig. 2(a), the maximum amount of CA release reached about 37% in the presence of Hyal as the amount of CA release was negligible without Hyal. The obvious difference demonstrated the important role of Hyal in the "on-demand" drug release. In addition, the photothermal-promoted drug release was studied. As was hypothesized, the photothermal effect of the vehicle accelerated and enhanced the release of CA both in the presence or absence of Hyal (Fig. S7 in the ESM). Then, Hyal-triggered CA release was further confirmed. As shown in Fig. 2(b), when heat-denatured Hyal was added into CA@AuMN-HA solution, low amount of CA release was observed. Furthermore, nearly no drug release could be observed in the first 3 h, then when Hyal was added to the acetate buffer 3 h after CA@AuMN-HA immersion, the release of CA increased. Thus, HA capping not only minimized the CA leakage, but also endowed the system with enzyme-controlled "on-demand" release property, which would significantly improve the specific antibacterial effect of CA.

Encouraged by the efficient photothermal effect and the favorable CA-loading capability of AuMN-HA, the chemo-photothermal synergistic effects of CA@AuMN-HA against MDR bacteria were investigated, considering that the gram-positive bacteria could produce Hyal and secrete it to the extracellular periphery [36]. MRSA was chosen as the model bacteria to study the *in vitro* bactericidal ability of CA@AuMN-HA. Figure 3(a) gives a visual representation of MRSA incubated with different agents. The viability of MRSA was analyzed by optical density (OD) measurements in LB broth. As could be seen in Fig. 3(b), free CA, which had a concentration equivalent to that of CA@AuMN-HA, inhibited MRSA to a lesser degree when the viability of bacteria incubated with CA@AuMN-HA decreased by nearly 50%. This result indicated that compared with the free form of CA at an equivalent concentration, CA@AuMN-HA showed a greatly enhanced antibacterial effect. Meanwhile,

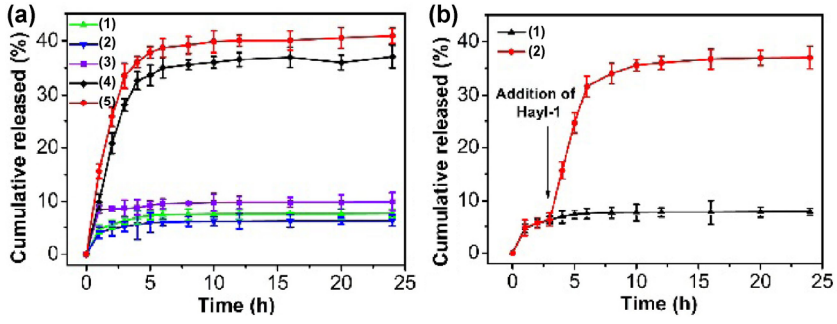

Figure 2 (a) Release profiles of CA from CA@AuMN-HA (1) acetate buffer (pH = 5), (2) PBS buffer (pH = 7.4), (3) acetate buffer with NIR irradiation for 5 min, (4) acetate buffer with Hyal, and (5) acetate buffer with Hyal and NIR irradiation for 5 min. (b) (1) Response of the AuMN-HA to the deactivated enzyme and (2) delayed release of CA from AuMN-HA by addition of Hyal after incubation for 3 h.

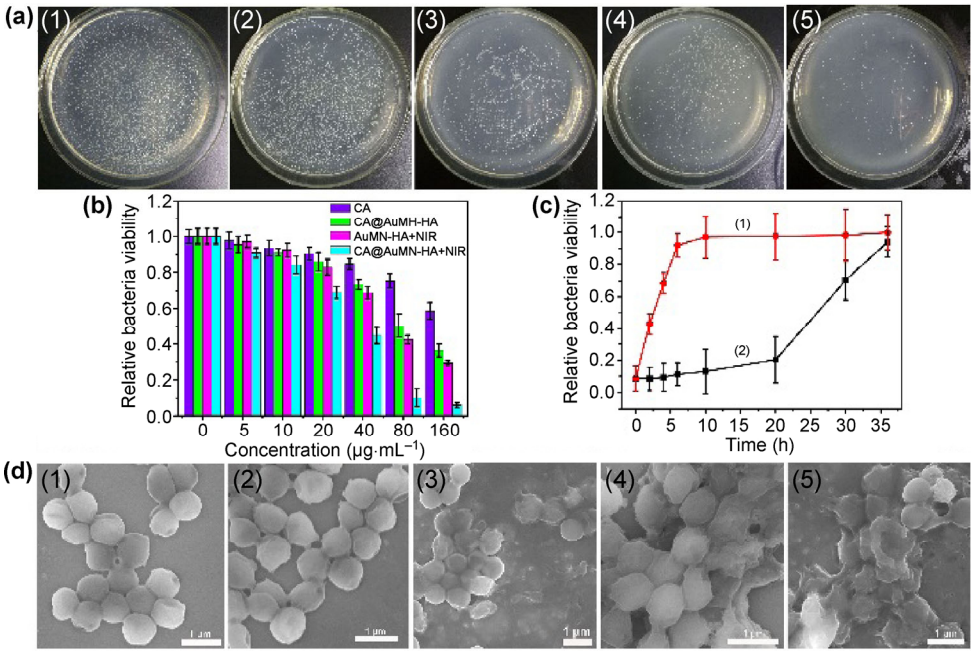

Figure 3 (a) Photographs of colonies formed by MRSA and (d) SEM images of MRSA after exposure to (1) PBS, (2) free CA, (3) CA@AuMN-HA, (4) AuMN-HA + NIR, and (5) CA@AuMN-HA + NIR. (b) Survival rates of MRSA strain at different concentrations of free CA, CA@AuMN-HA, AuMN-HA + NIR, and CA@AuMN-HA + NIR. (c) The growth curves of MRSA treated with (1) PBS buffer (pH = 7.4) and (2) 160 μg·mL^{-1} CA@AuMN-HA+NIR for 36 h. NIR irradiation: 2.5 W·cm^{-2} for 5 min.

the viability of MRSA incubated with AuMN-HA under NIR irradiation decreased by 57%. Moreover, the inhibition ratio reached up to 90% when MRSA was incubated with CA@AuMN-HA (80 μg·mL^{-1}) and exposed to 808 nm laser. This notable bacterial inactivation ability might be attributed to the combination of chemotherapy and photothermal therapy. To further decipher the bactericidal behavior, SEM images were acquired to observe the morphological changes in bacteria after treatment with various bactericidal agents (Fig. 3(c)). Furthermore, CA@AuMN-HA was found to possess good antibacterial efficacy for a long duration (Fig. 3(d)). Additionally, drug-resistant gram-negative *E. coli* was treated with CA@AuMN-HA. Since gram-negative bacteria mainly secrete periplasmic enzymes [35], the capping agent could not be destroyed effectively. As expected, CA@AuMN-HA displayed minor bactericidal effect (Fig. S8 in the ESM), which proved that our system could prevent undesired leakage of CA without the Hyal-secreting bacteria. In short, the CA@AuMN-HA-based bactericidal system would greatly enhance

the bioavailability and selectivity of CA. Meanwhile, the antibacterial ability was significantly improved due to the synergistic effect of chemotherapy and photothermal therapy.

Finally, we assessed the *in vivo* antibacterial ability of the designed system by utilizing mouse models of bacteria-infected wounds on their back. Twenty BALB/c mice were divided into five groups to develop the wound healing models. The MRSA-infected wounds of the mice were topically treated with different agents. As depicted in Fig. 4, obvious purulence was observed in the control and free CA-treated groups after 3-day treatment, while the wounds in the other three groups did not putrefy. Notably, compared with those in the other groups, the mice treated with the synergistic system (CA@AuMN-HA + NIR) showed much smaller wound size and tended to recover. In addition, H&E staining was employed to evaluate the wound healing process. On the third day, numerous inflammatory cells migrated to the wound site and a fragmented epidermal layer was formed on the wounds in control and free CA treated groups. In contrast, at the wound site on the mice in the synergistic system-treated group, less inflammatory cells appeared and an intact epidermal layer was formed (Fig. 4). To confirm the *in vivo* bactericidal effect, the wound tissues were excised to quantify the bacterial count (Fig. S9 in the ESM). From the grown colonies, we could clearly observe that compared with the control groups, the synergy system-treated group exhibited the most potent antibacterial effect and wound healing ability (Fig. S10 in the ESM). In brief, all the *in vivo* experiments proved that the synergistic antibacterial system possessed the most potent bactericidal effect and wound healing ability, offering a novel strategy for the treatment of MRSA infection.

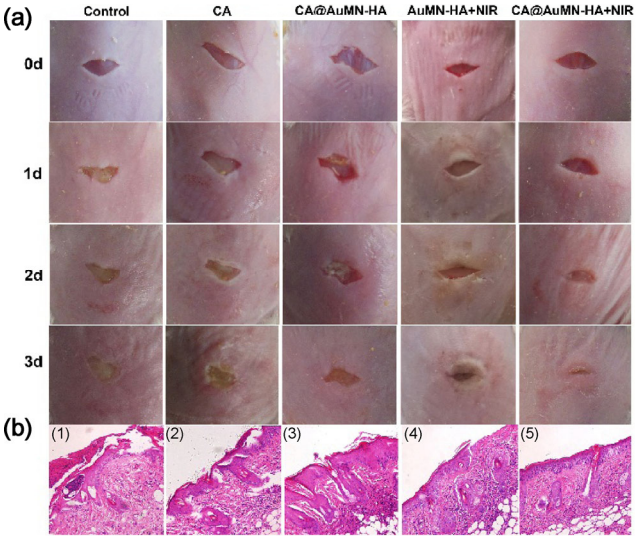

Figure 4 (a) Photographs of MRSA-infected wounds on mice in different treatment groups within 3 days. (b) Histological examination of the skin tissue slices by H&E staining. The skin tissue samples from groups (1)–(5) were topically treated with PBS buffer, free CA, CA@AuMN-HA, AuMN-HA + NIR, and CA@AuMN-HA + NIR, respectively.

To further explore the potential of the bactericidal system for clinical applications, biocompatibility and biosafety of CA@AuMN-HA were studied. Firstly, a MTT assay was performed to evaluate the toxicity of the system in MC-3T3-E1 cells. After incubating with increasing concentrations of CA@AuMN-HA for 24 h, the cell viabilities were only slightly influenced even at the high concentration of 320 $\mu g \cdot mL^{-1}$ (Fig. S9 in the ESM). Then, a histological analysis of the six major organs that were harvested from the sacrificed mice after the 3-day topical treatment was performed by H&E staining. Compared with the images from normal mice, the synergistic system revealed no appreciable histological abnormalities or damages to these organs after 3 days of treatment (Fig. 5). Thus, it could be concluded that the synergistic system possessed excellent biocompatibility and was essentially nontoxic to the treated mice during the treatment of bacterial infection.

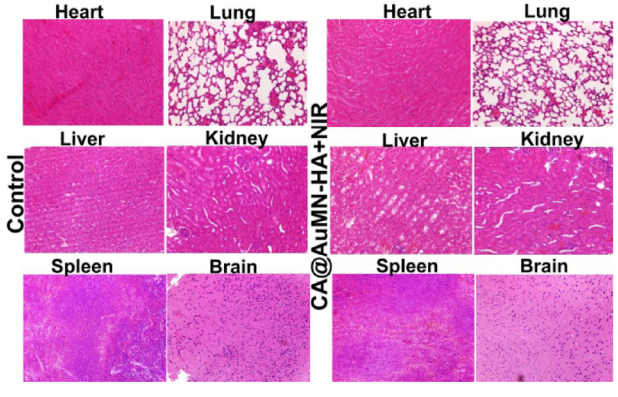

Figure 5 Pathological analysis of the cytotoxic effect caused by CA@AuMN-HA + NIR on the major organs (heart, liver, spleen, lung, kidney, and brain).

4 Conclusions

In summary, for the first time, a novel "on-demand" phytochemical delivery nanoplatform was constructed to treat the MDR bacterial infection. This nanoplatform (CA@AuMN-HA) would greatly enhance the bioavailability and selectivity of the encapsulated PEOs and significantly improve their bactericidal effect after combination with photothermal ability of the nanocarrier. Meanwhile, the synergistic system could effectively eliminate the drug-resistant bacteria with negligible biotoxicity. Given the increasing risk of antibiotic resistance, we believe this phytochemical-encapsulated nanoplatform would provide a long-term solution and be a new powerful tool for skin-associated bacterial infections.

Acknowledgements

We acknowledge financial support from the National Natural Science Foundation of China (Nos. 21210002, 21431007, 21533008, 21403209, 21601175, and 21673223) and the Jilin Province Science and Technology Development Plan Project (No. 20140101039JC).

Electronic Supplementary Material: Supplementary material (SEM images, TEM images, N_2 adsorption–desorption isotherms, UV–Vis spectra, plots of temperature increase, antibacterial assay of *E. coli* bacteria, MRSA bacteria number and colony separated from the wound tissue and the mammalian cytotoxicity of the nanoplatform) is available in the online version of this article at https://doi.org/10.1007/s12274-017-1947-y.

References

[1] Jones, K. E.; Patel, N. G.; Levy, M. A.; Storeygard, A.; Balk, D.; Gittleman, J. L.; Daszak, P. Global trends in emerging infectious diseases. *Nature* **2008**, *451*, 990–993.

[2] Li, L.-L.; Xu, J.-H.; Qi, G.-B.; Zhao, X. Z.; Yu, F. Q.; Wang, H. Core–shell supramolecular gelatin nanoparticles for adaptive and "on-demand" antibiotic delivery. *ACS Nano* **2014**, *8*, 4975–4983.

[3] Alanis, A. J. Resistance to antibiotics: Are we in the post-antibiotic era? *Arch. Med. Res.* **2005**, *36*, 697–705.

[4] Zhao, Y. Y.; Chen, Z. L.; Chen, Y. F.; Xu, J.; Li, J. H.; Jiang, X. Y. Synergy of non-antibiotic drugs and pyrimidinethiol on gold nanoparticles against superbugs. *J. Am. Chem. Soc.* **2013**, *135*, 12940–12943.

[5] Andersson, D. I.; Hughes, D. Microbiological effects of sublethal levels of antibiotics. *Nat. Rev. Microbiol.* **2014**, *12*, 465–478.

[6] Li, W.; Dong, K.; Ren, J. S.; Qu, X. G. A β-lactamase-imprinted responsive hydrogel for the treatment of antibiotic-resistant bacteria. *Angew. Chem., Int. Ed.* **2016**, *128*, 8181–8185.

[7] Chellat, M. F.; Raguž, L.; Riedl, R. Targeting antibiotic resistance. *Angew. Chem., Int. Ed.* **2016**, *55*, 6600–6626.

[8] Lewis, K. Platforms for antibiotic discovery. *Nat. Rev. Drug Discov.* **2013**, *12*, 371–387.

[9] Bai, H. T.; Lv, F. T.; Liu, L. B.; Wang, S. Supramolecular antibiotic switches: A potential strategy for combating drug resistance. *Chem.—Eur. J.* **2016**, *22*, 11114–11121.

[10] Campana, R.; Casettari, L.; Fagioli, L.; Cespi, M.; Bonacucina, G.; Baffone, W. Activity of essential oil-based microemulsions against *Staphylococcus aureus* biofilms developed on stainless steel surface in different culture media and growth conditions. *Int. J. Food Microbiol.* **2017**, *241*, 132–140.

[11] Duncan, B.; Li, X. N.; Landis, R. F.; Kim, S. T.; Gupta, A.; Wang, L.-S.; Ramanathan, R.; Tang, R.; Boerth, J. A.; Rotello, V. M. Nanoparticle-stabilized capsules for the treatment of bacterial biofilms. *ACS Nano* **2015**, *9*, 7775–7782.

[12] Landis, R. F.; Gupta, A.; Lee, Y.-W.; Wang, L.-S.; Golba, B.; Couillaud, B.; Ridolfo, R.; Das, R.; Rotello, V. M. Cross-linked polymer-stabilized nanocomposites for the treatment of bacterial biofilms. *ACS Nano* **2017**, *11*, 946–952.

[13] Amato, D. N.; Amato, D. V.; Mavrodi, O. V.; Braasch, D. A.; Walley, S. E.; Douglas, J. R.; Mavrodi, D. V.; Patton, D. L. Destruction of opportunistic pathogens via polymer nanoparticle-mediated release of plant-based antimicrobial payloads. *Adv. Healthcare Mater.* **2016**, *5*, 1094–1103.

[14] Wright, G. D. Opportunities for natural products in 21st century antibiotic discovery. *Nat. Prod. Rep.* **2017**, *34*, 694–701.

[15] Lewis, K; Ausubel, F. M. Prospects for plant-derived antibacterials. *Nat. Biotechnol.* **2006**, *24*, 1504–1507.

[16] Batish, D. R.; Singh, H. P.; Kohli, R. K.; Kaur, S. Eucalyptus essential oil as a natural pesticide. *Forest Ecol. Manag.* **2008**, *256*, 2166–2174.

[17] Isman, M. B. Plant essential oils for pest and disease management. *Crop Prot.* **2000**, *19*, 603–608.

[18] Liakos, I.; Rizzello, L.; Hajiali, H.; Brunetti, V.; Carzino, R.; Pompa, P. P.; Athanassiou, A.; Mele, E. Fibrous wound dressings encapsulating essential oils as natural antimicrobial agents. *J. Mater. Chem. B* **2015**, *3*, 1583–1589.

[19] Feng, K.; Wen, P.; Yang, H.; Li, N.; Lou, W. Y.; Zong, M. H.; Wu, H. Enhancement of the antimicrobial activity of cinnamon essential oil-loaded electrospun nanofilm by the incorporation of lysozyme. *RSC Adv.* **2017**, *7*, 1572–1580.

[20] Ramasamy, M.; Lee, J.-H.; Lee, J. Development of gold nanoparticles coated with silica containing the antibiofilm drug cinnamaldehyde and their effects on pathogenic bacteria. *Int. J. Nanomed.* **2017**, *12*, 2813–2828.

[21] Chan, A. C.; Bravo Cadena, M.; Townley, H. E.; Fricker, M. D.; Thompson, I. P. Effective delivery of volatile biocides employing mesoporous silicates for treating biofilms. *J. R. Soc. Interface* **2017**, *14*, DOI: 10.1098/rsif.2016.0650.

[22] Kim, B.; Lee, E.; Kim, Y.; Park, S.; Khang, G.; Lee, D. Dual acid-responsive micelle-forming anticancer polymers as new anticancer therapeutics. *Adv. Funct. Mater.* **2013**, *23*, 5091–5097.

[23] Gomes, C.; Moreira, R. G.; Castell-Perez, E. Poly (DL-lactide-co-glycolide) (PLGA) nanoparticles with entrapped trans-cinnamaldehyde and eugenol for antimicrobial delivery applications. *J. Food Sci.* **2011**, *76*, N16–N24.

[24] Noh, J.; Kwon, B.; Han, E.; Park, M.; Yang, W.; Cho, W.; Yoo, W.; Khang, G.; Lee, D. Amplification of oxidative stress by a dual stimuli-responsive hybrid drug enhances cancer cell death. *Nat. Commun.* **2015**, *6*, 6907.

[25] Mo, R.; Jiang, T. Y.; Di, J.; Tai, W. Y.; Gu, Z. Emerging micro- and nanotechnology based synthetic approaches for insulin delivery. *Chem. Soc. Rev.* **2014**, *43*, 3595–3629.

[26] Zhong, H.-J.; Lu, L. H.; Leung, K.-H.; Wong, C. C. L.; Peng, C.; Yan, S.-C.; Ma, D.-L.; Cai, Z. W.; Wang, H.-M. D.; Leung, C.-H. An iridium(III)-based irreversible protein–protein interaction inhibitor of BRD4 as a potent anticancer agent. *Chem. Sci.* **2015**, *6*, 5400–5408.

[27] Teplensky, M. H.; Fantham, M.; Li, P.; Wang, T. C.; Mehta, J. P.; Young, L. J.; Moghadam, P. Z.; Hupp, J. T.; Farha, O. K.; Kaminski, C. F. et al. Temperature treatment of highly porous zirconium-containing metal–organic frameworks extends drug delivery release. *J. Am. Chem. Soc.* **2017**, *139*, 7522–7532.

[28] Samanta, S. K.; Quigley, J.; Vinciguerra, B.; Briken, V.; Isaacs, L. Cucurbit[7]uril enables multi-stimuli-responsive release from the self-assembled hydrophobic phase of a metal organic polyhedron. *J. Am. Chem. Soc.* **2017**, *139*, 9066–9074.

[29] Chen, Y.; Chen, H. R.; Shi, J. L. *In vivo* bio-safety evaluations and diagnostic/therapeutic applications of chemically designed mesoporous silica nanoparticles. *Adv. Mater.* **2013**, *25*, 3144–3176.

[30] Yang, X. J.; Liu, X.; Liu, Z.; Pu, F.; Ren, J. S.; Qu, X. G. Near-infrared light-triggered, targeted drug delivery to cancer cells by aptamer gated nanovehicles. *Adv. Mater.* **2012**, *24*, 2890–2895.

[31] Ju, E. G.; Li, Z. H.; Liu, Z.; Ren, J. S.; Qu, X. G. Near-infrared light-triggered drug-delivery vehicle for mitochondria-targeted chemo-photothermal therapy. *ACS Appl. Mat. Interfaces* **2014**, *6*, 4364–4370.

[32] Shen, S.; Tang, H. Y.; Zhang, X. T.; Ren, J. F.; Pang, Z. Q.; Wang, D. G.; Gao, H. L.; Qian, Y.; Jiang, X. G.; Yang, W. L. Targeting mesoporous silica-encapsulated gold nanorods for chemo-photothermal therapy with near-infrared radiation. *Biomaterials* **2013**, *34*, 3150–3158.

[33] Song, Y.-R.; Choi, M.-S.; Choi, G.-W.; Park, I.-K.; Oh, C.-S. Antibacterial activity of cinnamaldehyde and estragole extracted from plant essential oils against *Pseudomonas syringae* pv. actinidiae causing bacterial canker disease in kiwifruit. *Plant Pathol. J.* **2016**, *32*, 363–370.

[34] Shen, S. X.; Zhang, T. H.; Yuan, Y.; Lin, S. Y.; Xu, J. Y.; Ye, H. Q. Effects of cinnamaldehyde on *Escherichia coli* and *Staphylococcus aureus* membrane. *Food Control* **2015**, *47*, 196–202.

[35] Ji, H. W.; Dong, K.; Yan, Z. Q.; Ding, C.; Chen, Z. W.; Ren, J. S.; Qu, X. G. Bacterial hyaluronidase self-triggered prodrug release for chemo-photothermal synergistic treatment of bacterial infection. *Small* **2016**, *12*, 6200–6206.

[36] Baier, G.; Cavallaro, A.; Vasilev, K.; Mailänder, V.; Musyanovych, A.; Landfester, K. Enzyme responsive hyaluronic acid nanocapsules containing polyhexanide and their exposure to bacteria to prevent infection. *Biomacromolecules* **2013**, *14*, 1103–1112.